BEHAVIOURS OF REINFORCED CONCRETE CONTAINMENT MODELS UNDER THERMAL GRADIENT AND INTERNAL PRESSURE

Y. AOYAGI, H. OHNUMA
Central Research Institute of Electric Power Industry, 1646 Abiko, Abiko-shi, Chiba, Japan

Y. YOSHIOKA, K. OKADA, M. UEDA
Takenaka Technical Research Laboratory, Takenaka Komuten Co., Ltd., 5-14, 2-chome, Minamisuna, Tokyo 136, Japan

SUMMARY

The provisions for design concepts in Japanese Technical Standard of Concrete Containments for Nuclear Power Plants require to take account of thermal effects into design. The provisions also propose that the thermal effects could be relieved according to the degree of crack formation and creep of concrete, and may be neglected in estimating the ultimate strength capacity in extreme environmental loading conditions.

This experimental study was carried out to clarify the above provisions by investigating the crack and deformation behaviours of two identical reinforced cylindrical models with dome and basement (wall outer diameter 160 cm, and wall thickness 10 cm). One of these models was hydraulically pressurized up to failure at room temperature and the other was subjected to similar internal pressure combined with the thermal gradient of approximately 40 to 50°C across the wall. Initial visual cracks were recognized when the stress induced by the thermal gradient reached at about 85% of bending strength of concrete used. The thermal stress of reinforcement calculated with the methods proposed by the authors using an average flexural rigidity considering the contribution of concrete showed good agreement with test results. The method based on the fully cracked section, however, was recognized to underestimate the measured stress. These cracks considerably reduced the initial deformation caused by subsequent internal pressure.

The transitional membrane rigidity development under the pressure is effectively estimated by the method shown in FIP-CEB Model Code. As the cracks propagate more closely by internal pressure, effective stiffness gradually decreased to that corresponding to the fully cracked section where contribution of tensile stress in concrete become negligible. Thermal effects showed also reduction because of its self-relieving characteristics. In such a loading condition, the calculated stress distribution according to ACI Specification 307-69 appeared to show good agreement with the test results. It was experimentally concluded also that the thermal effects played a negligible role in ultimate yielding strength capacity.

Taking the results obtained from the beam tests into consideration in addition to the above mentioned results, the provision of the Japanese Technical Standard, which stipulates that the flexural rigidity is allowed to be lowered down to 50 percent of elastical full section values in determining thermal stresses, seemed to be conservative. But the value could be much more decreased when large external tensile forces are acting such as load condition III.

1. Introduction

In design of a concrete containment vessel for a nuclear power plant, thermal loads should be taken into consideration, including such other external forces as dead load, internal pressures and/or seismic force. Thermal stress, however, is related to the rigidity of the vessel and can be relieved by the creep and development of cracks in the concrete of the vessel. This self-limiting characteristics of thermal effect should be reflected on rational design.

Various design concepts on thermal effects are adopted by foreign Codes. The provisions for design concept in the Japanese Technical Standards of Concrete Containment Vessel stipulate that thermal stress can be estimated regarding the Young's modulus of concrete as the half of its normally used value in the loading conditions I, II, and III, and that thermal effects on ultimate strength capacity can be neglected under the condition IV for safety analysis.

On the other hand, experimental study on those thermal effects seems to be insufficient to certify the appropriateness of those design requirements.

This study was carried out to survey experimentally the thermal effects by comparing the behaviours of two identical reinforced concrete containment models, one is hydraulically pressurized to failure and the other is subjected to internal pressure under simultaneous thermal gradients.

2. Test Models

2.1 Shape and Dimensions: The test model consists of basement, cylindrical wall and hemispheric dome (Fig.1). The basement is 30 cm thick and 2.4 m in outer diameter with a manhole for manufacturing works at its center. Cylindrical wall of 10 cm thick is widened by hunch near the basement to increase the bending strength capacity. At the top of hemispheric dome with the same wall thickness, a metal item is set to provide air vent.

Model 1 was subjected only to internal pressure, and Model 2 with the same dimensions and reinforcement as those of Model 1 was subjected to thermal gradient in addition to the internal pressure.

2.2 Reinforcement: The reinforcement in those models were decided to be below the allowable stress of 2000 kg/cm^2 for the cross-sectional forces obtained by finite element analysis at the design pressure of 4 kg/cm^2. Thermal effects were neglected in designing those models. Radial tie reinforcements were distributed around the top of the dome and the wall near the basement according to the Japanese design requirements. Those reinforcements are as shown in Fig.1.

2.3 Materials: Micro concrete with maximum 10 mm aggregate in size was used considering the shallow space and the small concrete cover to the reinforcement. It may be taken that those two models have approximately the same properties. (Compressive strength: 302 kg/cm^2, Young's modulus of elasticity: 30.4 x 10^4 kg/cm^2)

Deformed bar of 6 mm in diameter was used for reinforcement. (Yield

strength: 3340 kg/cm^2, ultimate strength: 5350 kg/cm^2, elongation: 30%)

3. Test Method

3.1 Test Equipment: Neoprene rubber sheet with thickness of 5 mm was attached to the inner surface of models to avoid leakage of pressurized water in models, up to the pressure at failure. Air compressor was used at a lower pressure (to 6 kg/cm^2) and plunger pump for higher pressure.

The temperature of water in Model 2 was controlled to form the intended thermal gradient in the wall through temperature control system. The outer surfaces of dome and wall were sprinkled with the water cooled to constant temperature.

3.2 Test Procedure: Model 1 was repeatedly pressurized as shown in Fig. 2 (b). The temperature difference between the inner and outer surfaces of shell concrete (ΔTg) were used in three combinations to the pressure level in Model 2. Five combination loading steps are shown in Fig.2 (a), (b).

3.3 Method of Measurement: To obtain strain distribution in the models, approximately 200 units of wire strain gages were attached to the reinforcement and concrete. Deformations in radial directions were measured at 8 cross sections. Temperature distribution in the wall and foundations was observed with the use of embedded thermocouples.

4. Test Results and Considerations

4.1 Strength Characteristics: Table 1 shows the cracking, yield and ultimate strengths of Models 1 and 2 comparatively.

In Model 1, initial vertical cracks developed at the mid-height of cylindrical wall, and horizontal cracks near the foundation simultaneously at an inner pressure (Pr) of 3.5 kg/cm^2. Cracks developed reticulately over the wall in proportion to the increase of pressure.

Reinforcement in hoop direction began to yield at 7.0 kg/cm^2 and this caused the yielding of vertical reinforcement. Both Models failed finally by punching shear around the through-hole at top of dome.

In Model 2, initial cracks developed during the thermal loading of STEP 1. Behavious under the subsequent pressure were similar to those of Model 1.

Yield strength of Model 2 slightly decreased in comparison with that of Model 1, especially in vertical reinforcement, because of the induced thermal stress. The pressure 7 kg/cm^2 in the initial yielding corresponds to approximately 90% of the calculated value, the yield in vertical direction occurred at a pressure lower than the estimated yield strength of 12 kg/cm^2. This reduction might be caused by the inclined crack formation under bi-axial tension[1)] and by the bending moment developed at the upper portion following the reduction in the rigidity in hoop direction.

No shearing stress acted in the dome according to the elastic analysis. Banerjee et al[2)], however says that the splitting of concrete due to high bond stresses could be occurred by crack formation near the top of the meridionally reinforced dome. The punching shear failure recognized in the test models is

thought to have been caused by the similar phenomenon. More studies on quantative estimating method of those strength and effectiveness of radial shear reinforcement seem necessary. Anyhow, it was clarified that the thermal effect played a negligible role on the ultimate strength.

4.2 Crack Characteristics

(1) Cracking strength: Comparing the measured cracking strengths in Models 1 and 2 with the calculated values expected by elastic analysis, it was concluded that the splitting tensile strength of concrete can be used for the prediction of membrane cracking strength against internal pressure, while 85 percent of the bending strength of concrete should be used to estimate the cracking strength due to the restrained thermal moment.

(2) Crack pattern and crack width: Fig.3 shows the development of crack width according to the pressure increase in Model 1 (full line) and Model 2 (broken line). From this observation, the effect of thermal gradient on crack width may be neglected as far as this test is concerned because restrained thermal moments were reduced considerably by the crack formations as mentioned later in 4.4.

Crack spacing calculated by FIP-CEB Model Code[3] is 8.8 cm, and the measured values while stable cracks are forming, are 8.7 cm, 9.5 cm in Models 1 and 2, respectively. And also, calculated crack width by the Code showed good agreement with the measured value as shown in Fig.3. Thus, the estimating method prescribed in CEP-FIP Model Code seems effective for crack analysis.

While cracks due to thermal gradient alone have a characteristic of being locally distributed compared with those by internal pressure. Therefore, another approach considering the relief of restrained moment seems necessary.

4.3 Deformation and Membrane Rigidity: The average rigidity reduced by crack formation does not readily reach that of reinforcement due to the contribution of remaining tensile stresses between the cracks. The various proposed methods to calculate the average strain (εsm) of reinforcement referring to the rigidity can be classified roughly as the following two equations.

$$\varepsilon sm = \frac{\sigma s}{Es}\left\{1-k\left(\frac{\sigma sr}{\sigma s}\right)^2\right\} \;\ldots\ldots\; (1)^{3),4)}, \quad \varepsilon sm = \frac{\sigma s}{Es}\left\{1-k\,\frac{\sigma sr}{\sigma s}\right\} \;\ldots\ldots\; (2)$$

Where, σs : stress of reinforcement

Es : Young's modulus of steel

σsr : σs immediately after the cracks were formed ($\sigma sr = \sigma ct / p$ when actual tensile force are eminent, σct : tensile strength of concrete, p: reinforcement ratio)

k : constants different from the loading conditions or arrangement of reinforcement

Fig.4 shows the observed deformation under pressure (full line: Model 1 and broken line: Model 2) and the calculated ones at the mid-height of walls which are subjected to membrane tension force.

The initial rigidity of Model 2 when subjected to thermal load is reduced by about one-third in comparison with that of Model 1 due to the thermal

cracks, but in the region over the design pressure it was recognized that the thermal gradient have an effect to reduce deformation.

The observed deformation before crack formation approximately coincide with the calculated value ((A) in Fig.) due to elastic analysis. With the increase of pressure, the deformation of those models asymptotically approaches to the line (1) which neglects the existence of concrete. From this fact, eq. (1) is considered more adequate to estimate the deformation when comparing with the eq. (2). The curve (2), (3) in Fig.4 calculated from the next eq. (3) where constant (k) is set to 0.7 and 1.0, well agreed with the measured deformation.

$$\delta r = \varepsilon sm \cdot b = \frac{\sigma sb}{Es}\{1-k(\frac{\sigma ct}{p\sigma s})^2\}, \quad \sigma s = \frac{Pr \cdot a}{ph} \quad \ldots\ldots (3)$$

where a, b: inner and outer diameter of wall, h: wall thickness

4.4 Reduction of Thermal Loads from Strain Measurement

(1) Reinforcement stress due to thermal gradient: The calculating methods proposed to estimate the thermal moment or the stress distribution under thermal gradients fall into two main groups. One estimates the equivalent restrained thermal moment based on the reduced flexural rigidity of crack section [5], [6] (Method A), and the other on the average flexural rigidity considering the remained tensile stress in concrete such as the method proposed by the authors [7] [8] (Method B).

Fig. 5 shows the calculated stress development in the reinforcement due to the above mentioned methods, as well as the measured ones obtained from the strain gages near the thermal cracks observed during the Step 1 loading in Model 2.

The following conclusions are obtained from the comparison. The method [A] underestimates the thermal stress especially in the region where thermal loads are considerably small and cracks are not fully propagated.

The stress calculated by the method B gives a slight overestimating tendency but gives fairly good agreement with the test results. From the other viewpoints, the restrained thermal moment estimated by elastic analysis could be reduced by 30-40% due to the crack formation.

(2) Reduction of thermal moment caused by axial tensile force: At the mid-height of cylindrical wall of Model 2, the acting restrained thermal moment could be relieved by the axial tensile force due to internal pressure.

The bending moment could be obtained from the value by multiplying the distance between inner and outer reinforcement (d-d') with the remainder of respective tensile forces(P_1-P_2) across the cross section. Tensile forces (P_1, P_2) are given as solution of next eq. (4).

$$\varepsilon sm = \frac{P}{AsEs}\{1-k(\frac{Po}{P})^2\} \quad \ldots\ldots (4)$$

(obtained by substituting $P = As\sigma s$, $Po = As\sigma_{sr}$ into eq. (1)

where As : cross-sectional area of reinforcement

εsm : measured average strain of gages

Table 2 shows tensile forces and flexural moments estimated by the above mentioned method as well as the calculated ones.

This estimating method seems almost adequate from the comparison between the measured and calculated tensile forces. The restrained moments due to thermal gradient are reduced considerably to 15-30% of the elastically analysed value due to the flexural rigidity reduction accompanied by the axial forces. And those moments are dissipated when both reinforcement stresses reach yield strength.

This reduction factor obtained from the flexural beam tests carried out by one of the authors[9] shows a value greater than the above values owing to the absence of axial tensile forces.

Thus, the reduction factor 0.5 prescribed in the Japanese Technical Standards could be a little decreased if tensile axial forces are coexistent in the loading condition III.

(3) Reduction of restrained thermal moment in wall near the foundation:

Besides the restrained thermal moment (Mtg + Mtd, moment due to the gradient: Mtg, and the differential moment induced by the difference in temperatures between foundation and walls: Mtd), flexural moment and axial force due to internal pressure act in the wall near the basement.

Fig.6 (a) shows the moment distribution acting on Models 1 and 2 estimated by the previously mentioned method at internal pressure of 7 kg/cm^2 in which the stress in the reinforcement reached partially near the yield strength. The remainder in Models 1 and 2 is expected to be equal to the actually acting restrained moment (Mt = Mtd + Mtg). On the other hand, the moment distribution obtained from the FEM elastic analysis is given in Fig.6 (b).

It is recognized obviously from the comparison between those figures that the restrained thermal moments are remarkably relieved. In their loading conditions, the calculating method based on fully cracked cross section neglecting the existence of concrete could be applied to estimate restrained thermal moment.

5. Conclusions

The conclusions obtained from the test results are summarized as follows.

(1) Thermal gradient could give an effect on the yield strength of reinforced concrete containment when subjected to internal pressure, but play a negligible role on the ultimate strength or the behaviours after yield.

(2) Calculating method to determine the average rigidity or crack development under axial tensile force according to CEP-FIP MODEL CODE was considered effective.

(3) Calculating method of thermal stress distribution based on the flexural rigidity of cracked section could give an underestimated value when cracks are not fully propagated. The method using an average flexural rigidity considering the contribution of tensile stress of concrete proposed by the authors, gave a conservative estimation and showed fairly good agreement

with test results

(4) Restrained thermal moment is relieved remarkably by external cross-sectional forces. The reduction factor 0.5 prescribed in the Japanese Technical Standards may give a safety-side estimation, but considered to be able to decrease in the loading condition III.

From these tests, it is thought necessary to establish a design method for punching shear around the top of the dome or a calculating method to estimate crack characteristics due to thermal effect. Behaviours such as overall crack propagation or the strength of models could be estimated by elasto-plastic finite element analysis, but more detailed analysis considering the contribution of tensile stress of concrete may be necessary to explain the behaviours in the process when the cracks are developing.

References

1) Y.Aoyagi, K.Yamada, "An Experimental Approach to the Design of Network Reinforcement against In-Plane Shear in Reinforced Concrete Containments, 5-th SMiRT, Berlin, Germany, 1979.

2) A.K.Banerjee et al, "Design of Reinforced Concrete Containments," SMiRT, San Francisco, USA, August 1977.

3) International System of Unified Standard Codes of Practice for Structures, CEB-FIP Model Code for Concrete Structures, 3rd Edition, 1978.

4) P.S.Rao, "Trisegmental Moment-Curvature Relations for Reinforced Concrete Members," Journal of ACI, May 1973.

5) ACI COMMITTEE 307, "Specification for the Design and Construction of Reinforced Concrete Chimney (ACI307-69)," ACI, 1969.

6) G.Gurfinkel, "Thermal Effects in Walls of Nuclear Containments, Elastic and Inelastic Behavior," SMiRT, Berlin, Germany, Sept. 1971.

7) Y.Aoyagi, H.Onuma, "Experimental Study on the Cracking Behaviour of Reinforced Concrete Hollow Cylinders Subjected to Temperature Gradient," Review of the Thirtieth General Meeting, June 1976, The Cement Association of Japan.

8) T.Toki et al., "Experimental Study on the Behaviours of Reinforced Concrete Cylindrical Structures under Thermal Gradients," Takenaka Technical Research Report, Oct.1976.

9) K.Ichikawa, Y.Aoyagi, Y.Watanabe, "Design of Concept of Concrete Containment Vessels for Shear and Thermal Stresses," 5-th SMiRT, Berlin, Germany, 1979.

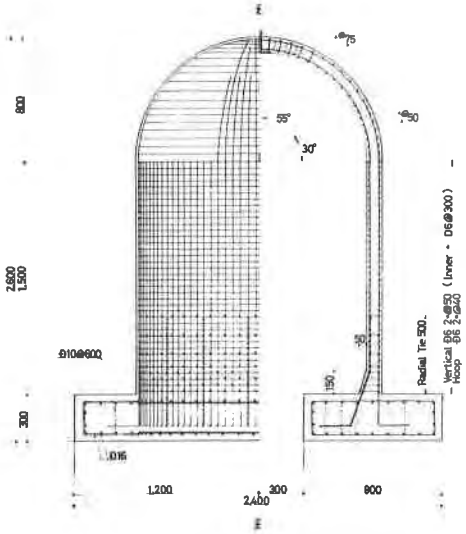

Fig.1 Test Model and Reinforcing Arrangement

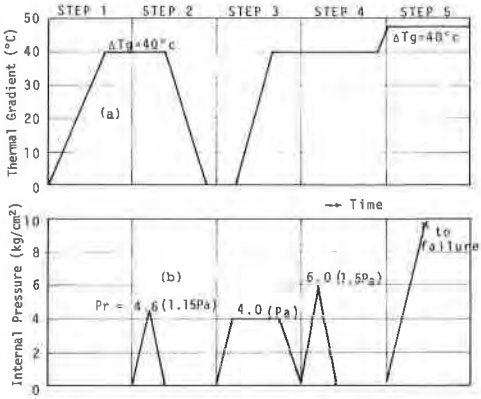

Fig.2 Loading Program
(Model 1: (b), Model 2: (a) + (b))

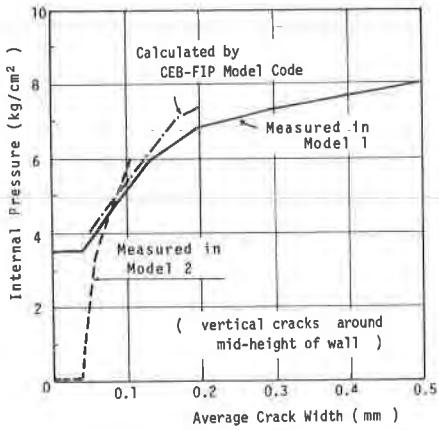

Fig.3 Development of Crack Width under Internal Pressure

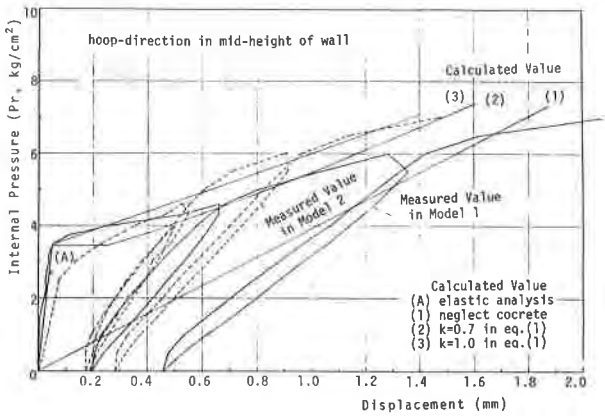

Fig.4 Comparison of Measured and Calculated Displacement under Internal Pressure

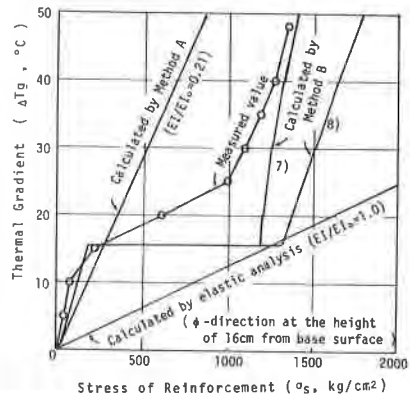

Fig.5 Development of Reinforcing Stress due to Thermal Gradient

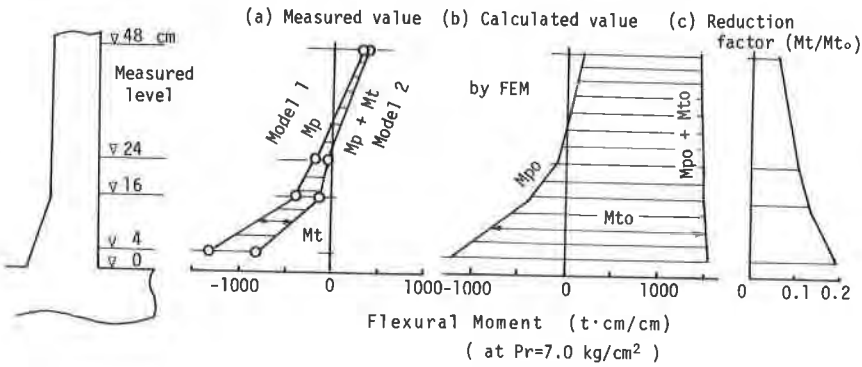

Fig.6 Moment Reduction around the Base-Wall Intersection

Strength	Location		Model 1	Model 2
Initial crack strength*	A	θ	Pr= 3.5	(ΔTg=20.3)
		φ	4.0	(20.3)
	B		3.5	(15.0)
	C		5.0	(20.3)
Yield strength*	φ	A	8.9	Pr= 7.9
		B	8.2	8.5
	θ	A	7.0	7.0
Ultimate strength	C		9.5	9.4

* from strain measurements

A: at mid-height of wall , B: at base-wall intersection, C: at dome

Table 1 Comparison of Strength in Model 1 and Model 2

Internal Pressure Pr (kg/cm²)	Measured value		Calculated value		Reduction factor (=M/Mo)	$P=P_1+P_2$ $M=(P_i-P_2)$ $*(d-d')$
	Normal force P (kg/cm)	Moment M(kg·cm/cm)	Normal force Po (kg/cm)	Moment Mo(kg·cm/cm)		
3.0	85	510	112	1040	0.490	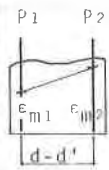
4.0	170	180	150	1040	0.173	
5.0	195	150	187	1040	0.144	
6.0	225	210	225	1040	0.202	
7.0	275	270	262	1248	0.216	
8.0	350	360	300	1248	0.288	

Table 2 Comparison of Measured and Calculated Moment, and Reduction Factor